Wavelength scaling of spiral patterns formed by granular media underneath a rotating fluid

F. Zoueshtiagh and P. J. Thomas*

Fluid Dynamics Research Centre, School of Engineering, University of Warwick, Coventry CV4 7AL, United Kingdom

(Received 27 September 1999; revised manuscript received 4 January 2000)

A spiral pattern formed by granular media underneath a rotating fluid is discussed. Results from a cellular-automaton model are compared to experimental data, and are found to reproduce experimentally observed scalings. A theoretical argument predicting these scalings on the basis of the existence of a critical threshold condition is advanced. It is suggested that the pattern is probably not associated with a hitherto unknown flow instability, as has been speculated previously. It appears that the pattern constitutes some rotating analog to sand ripples in nonrotating systems.

PACS number(s): 47.54.+r, 45.70.Qj, 47.55.Kf, 92.10.Wa

I. INTRODUCTION

A spiral pattern established in a granular layer underneath a rotating fluid is discussed. We first reported about the experimental observation of this pattern in Ref. [1], but were not able to present a conclusive explanation for the mechanism involved in the pattern formation. We did, however, speculate about a number of different possible such mechanisms. Here we will, for the first time, compare our experimental results to computational data. It will be found that a simple cellular-automaton model is sufficient to reproduce the characteristic scalings measured in the experiments. It will be shown that a simple intuitive theoretical argument can be advanced which can explain the scalings found experimentally and computationally. It will be argued that this result lends strong support to one of our hypothesis in Ref. [1] concerning the origin of the observed patterns.

In Ref. [1] we discussed a spiral pattern developing on the bottom of a partially fluid-filled, rotating tank (radius of tank $R = 44.75$ cm). The experimental setup is illustrated in Fig. 1. The bottom of the tank is initially covered with a thin layer (approximately 2–3 mm deep) of uniformly distributed granules. The fluid above the granule layer is in a state of solid-body rotation and, hence, does not move relative to the granules. Spiral patterns were observed to form when the rotational velocity of the tank is instantaneously increased from one constant rotation rate ω_0 to a higher rotation rate ω_1. The fluid mass in the tank cannot follow the instantaneous acceleration of the tank. This results in shear forces being established between the granule layer and the fluid above it. If the increment $\Delta\omega = \omega_1 - \omega_0$ is sufficiently large, such that the shear forces are high enough, then the granules are set in motion and begin to slide across the bottom of the tank. As a result of this, a reorganization process is initiated which leads to the formation of spiral patterns such as the one displayed in Fig. 2. Figure 2 shows the spiral pattern viewed from vertically above the tank. One can see spirals which were formed by the agglomeration of small (diameter around 0.3 mm) white granules against the black background of the tank. The patterns are fully established, typically,

10–20 sec after the spin-up of the tank. Patterns with between $7 \leq n \leq 110$ spiral arms were observed—refer to Ref. [1] for further photographs. The analysis of our experimental data in Ref. [1] revealed that

$$n \propto \frac{\omega_1^{0.5}}{\Delta\omega}. \tag{1}$$

Each of the spiral arms originates from an inner granule patch with a radius r_0. This inner patch appeared to remain essentially unaffected by the ongoing granule reorganization process. The radius of the inner patch was found to scale as

$$\frac{r_0}{R} = -0.34\ln\left(\frac{\Delta\omega}{\omega_c}\right) + 0.49 \tag{2}$$

for $0.4 \leq \Delta\omega/\omega_c \leq 3.5$. In Eq. (2), $\omega_c = 1.0$ rad s^{-1} is the measured critical rotational speed required to generate a pattern when the turntable is accelerated from rest ($\omega_0 = 0$).

It appears reasonable to assume that the force F_k required to set a granule in motion is constant everywhere on the granular layer on the bottom of the tank as long as centrifugal forces can be neglected. Hence the radius r_0 of the inner patch always corresponds to that location where the shear force exerted on the grains is equal to F_k. If one characterizes F_k in terms of some mean value v_k of the azimuthal flow velocity above the edge of the granule patch, then one expects

$$v_k = \text{const} \times \Delta\omega r_0. \tag{3}$$

Hence $r_0 \propto 1/\Delta\omega$, as was argued and verified experimentally in Ref. [1], where it was found that

$$\frac{r_0}{R} = 0.5\left(\frac{\Delta\omega}{\omega_c}\right)^{-1.05} \tag{4}$$

for $1.0 \leq \Delta\omega/\omega_c \leq 3.5$; i.e., when the data with lowest values of $\Delta\omega/\omega_c$ are neglected.

In the remainder we will computationally generate ripple patterns which will be found to display the $\Delta\omega$ scalings expressed by Eqs. (1) and (4). Facilitated by a comparison of the experimental and computational results, we will be enabled to arrive at certain conclusions concerning the origin and the physical mechanisms underlying the spiral-pattern formation first described in Ref. [1]. The discussion will, in
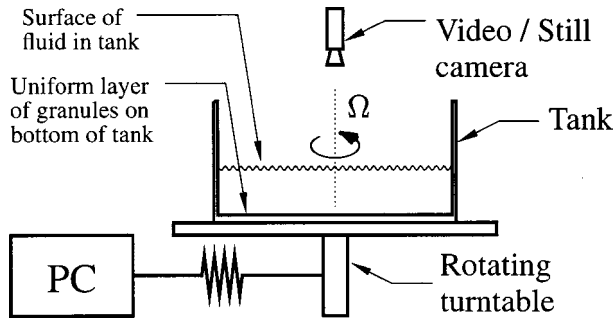

FIG. 1. Sketch of the experimental setup.

particular, suggest that the spiral patterns are not a visualization of, or associated with, a hitherto unknown flow instability associated with the boundary layer on the bottom of the tank, as has been suggested previously. On the basis of the results discussed here it will emerge that the spiral patterns appear to be some type of rotating analog of sand ripples such as commonly observed in similar form in the desert or on beaches.

II. COMPUTATIONAL APPROACH

The computational approach adopted to investigate the observed ripple patterns represents, essentially, an adaptation of the type of cellular-automaton model described, for instance, by Kaneko [2] or Nishimori and Ouchi [3]. Nishimori and Ouchi used such a model to simulate the formation of ripple patterns in an aeolian system of wind-blown sand in a straight channel. Here we will adapt and generalize this model to suit the circular flow geometry of our present experiment. It is noted that the particular mapping functions chosen in Ref. [3] to model grain transport were originally devised with aeolian systems in mind. In such systems the physical mechanisms involved in ripple formation are different than in fluvial system [4–7]. Nevertheless, it will be found that the model of Nishimori and Ouchi is sufficient to reproduce the essential scalings observed in our fluvial system. The discussion of this observation will reveal that it is not, in fact, the details of the mapping functions employed to simulate grain transport that are important, but rather the existence of a critical threshold condition inherent in the model. On the basis of this observation it will be possible to formulate appropriate physical arguments readily yielding the experimentally observed scalings. These physical arguments and the conclusions drawn from them appear to shed some first light on the origin of the spiral patterns and on some of the physical mechanisms involved in their formation. In this respect the present study constitutes, as far as we are aware of, probably the first direct application of the model of Nishimori and Ouchi to a real physical system.

For our adaptation of the model described in Ref. [3], we make the simplifying assumption that the fluid as well as the granules move in concentric circular trajectories around the center of the tank. Hence only the azimuthal velocity component v of the granules and the fluid is accounted for. The radial flow component, which exists in the physical system, is neglected. This assumption does, of course, represent a severe simplification of the flow in and above the Ekman boundary layer [8,9] over the loose granular boundary [10].
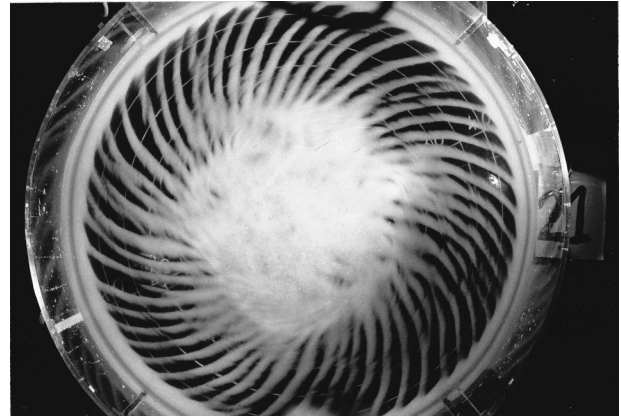

FIG. 2. Spiral-ripple pattern observed in an experiment with $\Delta\omega = 0.8$ rad s^{-1} and $\omega_1 = 3.1$ rad s^{-1}; the turntable rotates counter-clockwise. The diameter of the pattern corresponds to the diameter (89.5 cm) of the fluid-filled circular tank.

However, it will be seen that the assumption does not affect our main conclusions.

We assume a coordinate system, with coordinates x and y, which is fixed in the rotating frame of reference and whose origin coincides with the center of the rotating tank. The simulations are performed on a lattice with 200×200 grid points. The computational domain is initialized by random initial conditions according to $h(x,y) = h_0 + \delta$, where $h(x,y)$ specifies the height of the sand surface at site x,y, and where the random number δ is very small compared to the constant h_0. It is assumed that the azimuthal flow velocity $v(r)$ on neighboring concentric flow trajectories increases linearly with the distance r from the center of the tank, such that

$$v(r) = (\omega_1 - \omega_0)r = \Delta\omega r. \qquad (5)$$

Saltation and creep [3,4] are assumed to be the two mechanisms responsible for grain transport. The two mechanisms are modeled by moving grains around the lattice sites according to some simple mapping functions. The mapping proceeds from one iteration step n to step $n+1$ via an intermediate step n'. The saltation step is carried out first, and the result is stored as the intermediate step n'. Then the creep step is performed to yield the final result for time step $n+1$.

Saltation is described by moving a number of q granules over a certain saltation flight length $L(r)$ from one grid position to another one. With regard to the circular flow geometry we interpret $L(r)$ as an arc with radius $r = \sqrt{x^2 + y^2}$. The flight length $L(r)$ has, thus, components L_x and L_y in both coordinate directions. The values of L_x and L_y associated with $L(r)$ can be determined from simple geometric considerations. The flight length is modeled as

$$L(r) = L_0(r) + b(r)[h_n(x,y) - h_0]. \qquad (6)$$

In Eq. (6) $L_0(r)$ is a control parameter assumed to represent the shear stress imposed on the sand surface by the fluid moving above it. The appropriately nondimensionalized quantity $b(r)$ is assumed to represent the mean flow velocity experienced by a grain during its saltation flight. The physical meaning of the term $[h_n(x,y) - h_0]$ is that the flight
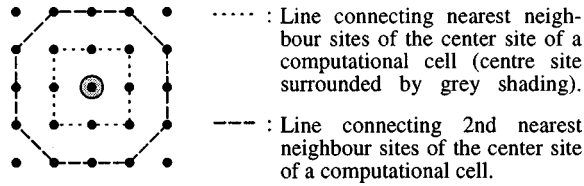
FIG. 3. Sketch illustrating the definition of nearest and second-nearest-neighbor sites underlying the computations.

length of a grain will be the longer the higher its starting point. With respect to the assumed linear radial increase of the azimuthal flow velocity, defined by Eq. (5), we scale $b(r)$ of Eq. (6) as $b(r)=b_0(\Delta\omega r/\Delta\omega R)$, where b_0 is a constant. A similar assumption is made for the value of $L_0(r)$ which is taken as $L_0(r)=k(\Delta\omega r/\Delta\omega R)\Delta\omega$, where, k is a constant. Finally, the actual saltation step by which the q granules are moved is summarized by the expressions

$$h_{n'}(x,y)=h_n(x,y)-q, \tag{7a}$$

$$h_{n'}(x+L_x(h_n),y+L_y(h_n))=h_n(x+L_x(h_n),y+L_y(h_n))+q. \tag{7b}$$

Note that we have abbreviated $h_n(x,y)$ as h_n in Eq. (7b) for simplicity.

The creep step is described as

$$h_{n+1}(x,y)=h_{n'}(x,y)+D\left[\frac{1}{8}\sum_{NN}h_{n'}(x,y)\right.$$
$$\left.+\frac{1}{12}\sum_{2ndNN}h_{n'}(x,y)-2h_{n'}(x,y)\right]. \tag{8}$$

In Eq. (8), the index notations NN and $2nd$NN indicate that the summations extend over the nearest and the second nearest neighbors, respectively. Our definition of nearest and second nearest neighbor sites is illustrated in Fig. 3, and differs from the definition used in Ref. [3]. Note that the last term on the right hand side of Eq. (3) of Ref. [3] is, in fact, incorrect as a factor 2 has been omitted. The term has to read correctly $\cdots -2h_{n'}(x,y)$ as in the above Eq. (8). We have verified that mass is conserved throughout the computations. As $L(r)\to 0$ for $r\to 0$, the grid structure will necessarily begin to affect the computations below some critical value of r. We have also observed some evidence of the square grid structure being visible in a number of our computational patterns for lower r. By performing computations on computational domains with different sizes, we have verified that our main quantitative results are not influenced by the actual domain size. In the remainder it will further be seen that mass conservation, the exact grid structure, and details of the algorithms underlying our computations are not, in fact, critical factors affecting our main conclusions.

III. COMPARISON OF COMPUTATIONAL AND EXPERIMENTAL DATA

Figures 4(a) and 4(b) show two different patterns obtained from our computations for values $\Delta\omega=5$ and $\Delta\omega=11$, respectively. Note that for the computations $\Delta\omega$ is specified in arbitrary units and not in units of rad s^{-1} as for the experi-
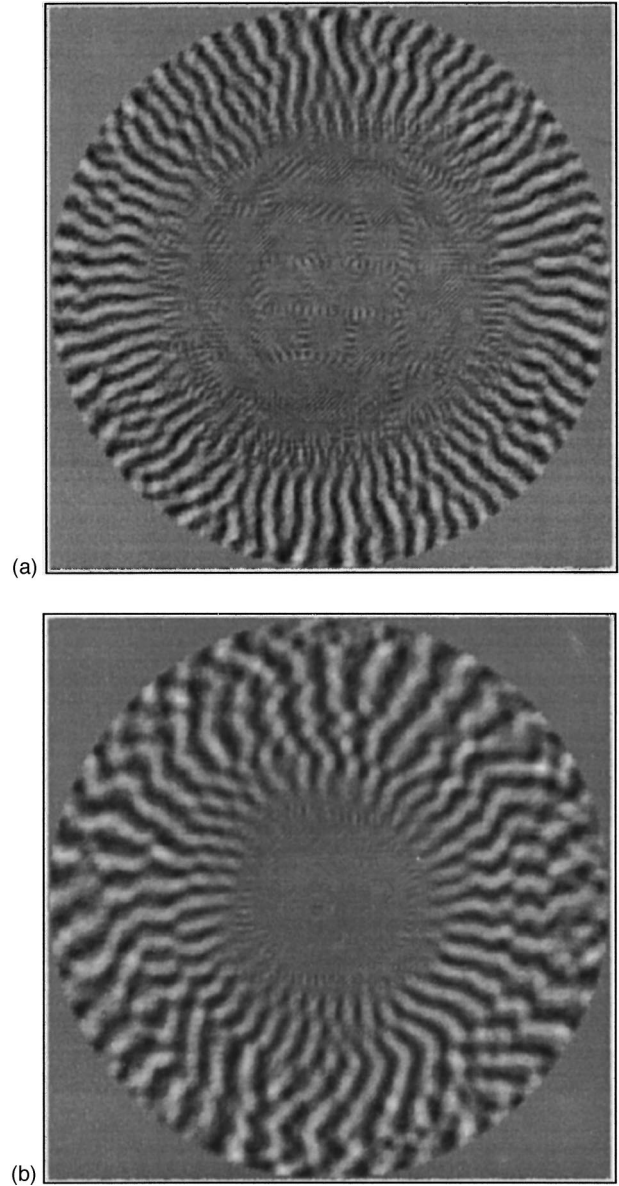

FIG. 4. Computational ripple patterns for two different values of $\Delta\omega$ specified in arbitrary units (a) $\Delta\omega=5$ and (b) $\Delta\omega=11$. For a comparison with the experimental pattern of Fig. 2 the diameter of the computed patterns should be equated with the diameter (89.5 cm) of the fluid-filled circular tank used in the experiment.

mental data. The values of the constants appearing in Eqs. (6)–(8) are $q=1$, $b_0=2$, $k=1$, and $D=1$. This particular set of parameters was chosen as it resulted in well established, distinct patterns. Pattern formation is not observed for all possible combinations of values of the parameters. This is similar to the observations discussed in Ref. [3]. The gray scale in Figs. 4(a) and 4(b) characterizes the height of granules at a particular lattice point. Light gray corresponds to higher numbers of granules being stacked on top of each other, whereas dark gray identifies lower values. The main qualitative aspects to note from Figs. 4(a) and 4(b) are as follows. The program produces a ripple pattern displaying a decreasing number of arms for increasing $\Delta\omega$. The arms originate from an inner patch whose radius decreases with increasing $\Delta\omega$. These results are consistent with the experimental observations. The pattern does, of course, not reveal a
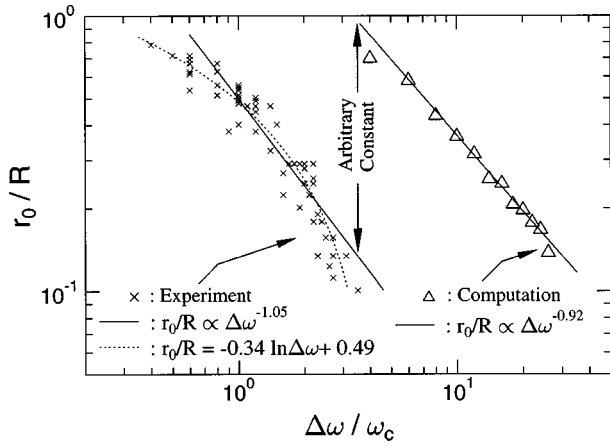
FIG. 5. Comparison of the inner patch radius observed in the experiments with the patch radius generated by the computations.

FIG. 6. Comparison of the number of spiral arms observed in the experiment with the number of ripples generated by our computations.

spiral structure as our model neglects the centrifugal force, the associated radial flow component and Coriolis effects. We have carried out a number of preliminary test runs which incorporated a radial flow component, and these produced a spiral pattern. It will, however, be found that the actual spiral structure is irrelevant in the present context.

Figure 5 shows a quantitative comparison between computational and experimental results for the diameter of the inner granule patch. It is estimated that the patch radius r_0/R can be determined with a maximum error of less than ± 0.04 from figures such as Figs. 4(a) and 4(b). When viewing Fig. 5, recall that $\Delta \omega$ is expressed in arbitrary units for the computations.

In Ref. [1], a best fit to the experimental data points according to Eq. (2) was obtained when a least squares fit is based on the entire data set displayed in Fig. 5. This fit is represented in Fig. 5 by the dotted line interpolating the experimental data points. However, it was argued above and in Ref. [1] that a power-law scaling according to $r_0/R \propto \Delta \omega^{-1}$ should be expected under the conditions discussed in connection with Eqs. (3) and (4). In Ref. [1] it was indeed verified that such a power-law fit is the best fit to the data points in the interval $1.0 \leqslant \Delta \omega/\omega_c \leqslant 3.5$. The fit based solely on the data points lying within this data interval is given by Eq. (4), and it is represented in Fig. 5 by the solid line through the experimental data points. A least-squares fit of power-law type through the computational data points of Fig. 5 yields $r_0/R \propto \Delta \omega^{-0.92}$. This result is in close agreement with the expected $\Delta \omega^{-1}$ scaling. For the data fit, the computational point with the lowest value of $\Delta \omega$ in Fig. 5 was neglected. The computations indicate that the $\Delta \omega^{-1}$ scaling breaks down for larger values of r_0/R. It appears that this is a consequence of the boundary conditions, associated with the finite computational domain, increasingly affecting the computations. Low values of $\Delta \omega$ are associated with a large inner patch. The edge of the patch is, thus, close to the system boundary. Hence the pattern formation process at the edge of the patch will be affected by inhomogeneities arising from the creep step of Eq. (8) in association with the finite computational domain. If the computational data point with the lowest value of $\Delta \omega$ is included in the least-squares fit, one finds $r_0/R \propto \Delta \omega^{-0.80}$. The experimental and computational data do, of course, differ by an arbitrary constant, as
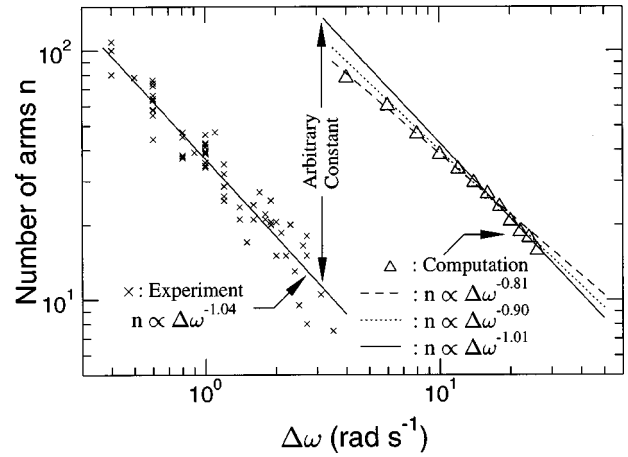
indicated in Fig. 5. The computations cannot, obviously, yield a physically correct value for this constant. In the physical system the constant should depend on the particular type of grains, on their size, and on the type of fluid used. These factors are not accounted for in the computations.

Figure 6 displays a comparison between the number of arms observed in the patterns generated by the computations and the number of spiral arms observed in the experiments. The experimental data, originally contained in Ref. [1], scale as $n \propto \Delta \omega^{-1.04}$. The number of arms of the computational patterns was counted in the immediate vicinity of the edge of the inner patch. Hence it does not take into account variations due to dislocations which appear occasionally at locations further radially outward from the edge of the patch. As discussed in the context of Fig. 5, data points for low values of $\Delta \omega$ appear to be influenced by affects arising from the finite computational domain. In order to account for this, Fig. 6 shows three different least-squares fits of power-law type to the computational data. These three alternative fits are intended to provide some means to evaluate the error associated with the exponent of the $\Delta \omega$ scaling. The dashed line represents a fit which takes account of all 12 data points shown and for which $n \propto \Delta \omega^{-0.81}$. The dotted line represents a fit for which the data points with the three lowest values of $\Delta \omega$ were neglected, and for which $n \propto \Delta \omega^{-0.90}$. The solid line represents a fit for which the data points with the five lowest values of $\Delta \omega$ were neglected, and for which $n \propto \Delta \omega^{-1.01}$. It can be concluded that the computational data are in excellent agreement with the experimental results.

IV. DISCUSSION AND CONCLUSION

The close agreement between the scalings observed in the experiment and in the computations prompted us to wonder what aspect of the model might, in fact, be responsible for this result. Evidently, the simple mapping functions employed to simulate grain motion cannot capture the details of the complicated physics of the small-scale grain dynamics on the bottom of the tank. Hence it appeared unlikely that the agreement between experiment and computation was a consequence of these particular functions. This observation led to the conclusion that the agreement was, in fact, a result of

critical threshold conditions which are inherent in both the physical system and the computational model. On the basis of this result it is then possible to formulate simple, intuitive physical arguments which readily yield the scalings observed in the experiment and the computations. These arguments are briefly summarized below. In this context it will become apparent what exactly is meant by critical threshold conditions.

As discussed in Sec. I, it is reasonable to assume that for one particular type of granules and one particular fluid, a certain constant critical force F_k is required to set a grain in motion. From Eqs. (3) it is known that this implies $r_0 \propto 1/\Delta\omega$, as was verified experimentally by Eq. (4). However, a constant F_k also suggests that the established azimuthal pattern wavelength λ_0 at the edge of the inner patch should be constant. Although the exact value of λ_0 is, of course, not known it is reasonable to assume that this wavelength will be the same no matter how large the patch radius r_0 is. Thus a necessary condition at the edge of the patch is consequently $2\pi r_0 = n\lambda_0$. Replacing r_0 in this expression by means of Eq. (3) readily yields $n = \text{const} \times (2\pi v_k/\lambda_0\Delta\omega)$. Hence $n \propto 1/\Delta\omega$, as is observed in the experiments—see Eq. (1). Thus the close agreement between experiment and computation appears to be a consequence of the existence of the critical force F_k necessary to set a granule in motion. In the computations this critical force corresponds to the existence of some critical value of $L_k(r)$ required to induce a ripple formation. The existence of this critical value has been verified theoretically as well as on the basis of computational data in Ref. [3]. Theoretically it follows from the stability analysis contained in Ref. [3]; computationally it is expressed by the phase diagram displayed in Fig. 3 of Ref. [3].

Originally it was the comparison between the experimental and the computational data which prompted us to realize the discussed physical arguments yielding the required scalings. In retrospect it appears, however, that the significance of the computational model in the context of this paper is, in fact, to support just these physical arguments. Whatever, the main conclusions of our discussions are as follows. The $\Delta\omega^{-1}$ pattern scaling first described in Ref. [1] can be understood in terms of the circular flow geometry together with a critical threshold condition. The actual granule motion as

such is, thus, irrelevant for the scalings observed in the experiments and expressed by Eqs. (1) and (4). Consequently, the number of spiral arms should not depend on the roughness of the bottom of the tank, as was speculated in Ref. [1]. The roughness restricts the motion of the grains and will, if at all, only affect the spiraling angle of each spiral arm. In Ref. [1] we suggested different incompatible hypotheses concerning the possible origin of the spiral patterns. One hypothesis was that the spiral patterns are a visualization of a hitherto unknown flow instability of the boundary layer flow on the bottom of the tank. The results obtained from our adaptation of the model described in Ref. [3] together with our physical arguments show, however, that our experimental observations do not necessitate postulating such a new instability. On the basis of these results it is concluded that the spiral patterns are probably not a visualization of, or associated with, a new flow instability. It now appears that the spiral patterns represent some type of rotating analog similar to such ripple patterns, as typically observed in sand on the bottom of the ocean or in the desert.

Although our results explain the scaling associated with the number of spiral arms observed, it still appears surprising that the arms indeed form outside the inner patch for $r > r_0$. As the photo of Fig. 2 reveals, there are large areas between neighboring spiral arms which are entirely free of granules. During the pattern formation process the granules slide across the bottom of the tank in these regions. One would expect the dynamics in the granule-free regions to be different from those on top of a granular layer. Hence it is not obvious why ripple patterns persist in the granule-free regions.

We have so far not been able to find a similarly simple physical argument to explain the $\omega_1^{1/2}$ scaling expressed by Eq. (1). However, with regard to our present results, it appears that this scaling cannot be a result of the Coriolis forces acting on the moving grains. Through the critical force F_k the number of spiral arms is effectively selected prior to the onset of the granule motion. The Coriolis force cannot, however, influence the dynamics until the granules move. Hence it appears reasonable to speculate that the $\omega_1^{1/2}$ scaling possibly reflects some influence of the centrifugal forces on the value of F_k.

---

[1] P. J. Thomas, J. Fluid Mech. **274**, 23 (1994).
[2] K. Kaneko, *Simulating Physics with Coupled Map Lattices*, Formation, Dynamics and Statistics of Patterns Vol. 1, edited by K. Kawasaki, M. Suzuki, and A. Onuki (World Scientific, Singapore, 1990), pp. 1–54.
[3] H. Nishimori and N. Ouchi, Phys. Rev. Lett. **71**, 197 (1993).
[4] R. A. Bagnold, *The Physics of Blown Sand and Desert Dunes* (Methuen, London, 1941).
[5] R. E. Hunter, Sedimentology **24**, 361 (1977).
[6] N. Lancaster, *Geomorphology of Desert Dunes* (Routledge,

London, 1995).
[7] J. R. L. Allen, *Sedimentary Structures* (Elsevier, Amsterdam, 1984).
[8] H. P. Greenspan, *The Theory of Rotating Fluids* (Cambridge University Press, Cambridge, England, 1968).
[9] J. M. Owen and R. H. Rogers, *Flow and Heat Transfer in Rotating-Disc Systems Volume 1, Rotor-Stator Systems* (Research Studies Press, Taunton, 1989).
[10] A. J. Raudkivi, *Loose Boundary Hydraulics*, 3rd ed. (Pergamon Press, Oxford, 1990).